Photochromic mechanism in oxygen-containing yttrium hydride thin films: An optical perspective

J. Montero,[1,][*] F. A. Martinsen,[1] M. García-Tecedor,[2] S. Zh. Karazhanov,[1] D. Maestre,[2] B. Hauback,[1] and E. S. Marstein[1]

[1]*Institute for Energy Technology, P.O. Box 40, NO-2027 Kjeller, Norway*
[2]*Complutense University of Madrid, Avenida Complutense, s/n, ES-28040 Madrid, Spain*

Oxygen-containing yttrium hydride thin films exhibit photochromic behavior: Transparent thin films reversibly switch from a transparent state to a photodarkened state after being illuminated with UV or blue light. From optical spectrophotometry and ellipsometry measurements of the transparent state and photodarkened state, it is concluded that the photochromic effect can be explained by the gradual growth, under illumination, of metallic domains within the initial wide-band-gap semiconducting lattice. This conclusion is supported by Raman measurements.

Oxygen-containing yttrium hydride films exhibit photochromic (PC) behavior, i.e., the optical properties of the films change reversibly when illuminated by light of adequate energy (wavelengths in the blue or UV range). Early works by Hoekstra *et al.* [1] reported photoconductivity in yttrium hydrides at low temperature, and Ohmura *et al.* [2,3] accidentally discovered PC behavior in yttrium hydride films subjected to high pressure. In addition, Huiberts *et al.* observed for the first time the gasochromic behavior of yttrium hydride thin films [4]. Later, Mongstad *et al.* [5,6] reported PC behavior in transparent oxygen-rich yttrium hydride films under atmospheric conditions and at room temperature. In the latter case, however, the yttrium hydride films were directly obtained by reactive magnetron sputtering rather than by the subsequent hydrogenation of a predeposited metallic Y layer. Oxygen-rich yttrium hydride is not the only oxygen-containing hydride which exhibits interesting physical properties. For instance, Miniotas *et al.* have reported gigantic resistivity and band-gap changes in oxygen-containing gadolinium hydride [7].

The mechanism of the PC behavior in oxygen-rich yttrium hydride is still unclear and seems to have no relation to the PC mechanism reported for transition-metal oxides [8]. In the present Rapid Communication, the properties of oxygen-rich transparent semiconducting yttrium hydride thin films—hereafter referred to as $YH_xO_w^{sc}$, where the superscript *sc* refers to their semiconducting character—and of opaque metallic yttrium hydride thin films—from now on referred to as $YH_yO_z^m$, where $y < x$ and where the superscript *m* refers to their metallic character—have been investigated by grazing incidence x-ray diffraction (GIXRD), Raman spectroscopy, ellipsometry, and spectrophotometry. Both sets of films, $YH_xO_w^{sc}$ and $YH_yO_z^m$, were deposited onto soda-lime glass substrates by sputter deposition at a hydrogen/argon ratio $\Gamma = 0.18$ and 0.13, respectively, and then exposed to air where they oxidize. A detailed description of the deposition method can be found in our previous work [9]. The $YH_xO_w^{sc}$ and $YH_yO_z^m$ films present a thickness of 690 and 580 nm, respectively, as determined by profilometry. The modeling of the experimental results revealed that the optical properties

of the $YH_xO_w^{sc}$ films in their photodarkened state (in this case achieved by using a broadband light source EQ-99XFC LDLS with an intense UV component) can be quantitatively explained by the formation of metallic $YH_yO_z^m$ domains embedded into the $YH_xO_w^{sc}$ (clear) matrix, according to the Maxwell-Garnett effective medium approximation [10]. These results are supported by preliminary Raman measurements and by the recent work by Chandran *et al.* [8], which reports changes of the hydrogen species in oxygen-containing yttrium hydride after illumination, suggesting the release of electrons and the formation of a metallic phase.

Figure 1(a) shows GIXRD patterns—obtained by using Cu $K\alpha$ radiation at a fixed angle of incidence of $2°$ in a Bruker Siemens D5000 diffractometer—for both transparent-semiconducting $YH_xO_w^{sc}$ (upper panel) and opaque-metallic $YH_yO_z^m$ (lower panel) thin films. The diffractogram for the $YH_yO_z^m$ thin films correspond to a mix of fcc-YH_2 and hexagonal-$YH_{0.667}$ metallic phases [11], according to the standard patterns JCPDS 04-006-6935 and JCPDS 01-074-8440. Due to the proximity of the standard diffraction peaks corresponding to $YH_{0.667}$ and Y (JPCDS 00-033-1458, not shown), the presence of a metallic yttrium phase cannot be totally ruled out from the $YH_yO_z^m$ films. The main peak, observed at around $30°$, is formed by the contribution of the $YH_{0.667}$ and YH_2 phases in the [111] and [006] directions, respectively. The lattice parameter corresponding to the fcc cubic phase matches very well the YH_2 standard of 5.20 Å in the case of the $YH_yO_z^m$ films, but it is much higher, about 5.40 Å, for the $YH_xO_w^{sc}$ samples. As a result, the experimental diffraction peaks for $YH_xO_w^{sc}$ in the directions [311], [220], [200], and [111] are displaced towards smaller angles compared to the standard [see Fig. 1(a), upper panel]. The same peaks, however, are located at the expected positions according to the standard in the $YH_yO_z^m$ films [Fig. 1(a), lower panel]. The increase of the lattice parameter in the $YH_xO_w^{sc}$ films has been observed before and attributed to a high oxygen content in the lattice [6], a feature responsible for the band-gap opening and the high transparency observed in these films [9,12]. Apart from the peaks corresponding to oxygen-containing yttrium hydride, no other phases are observed in the diffractograms corresponding to the $YH_xO_w^{sc}$ samples. Therefore, and according to these observations, the oxygen content in the $YH_xO_w^{sc}$ films is expected to be
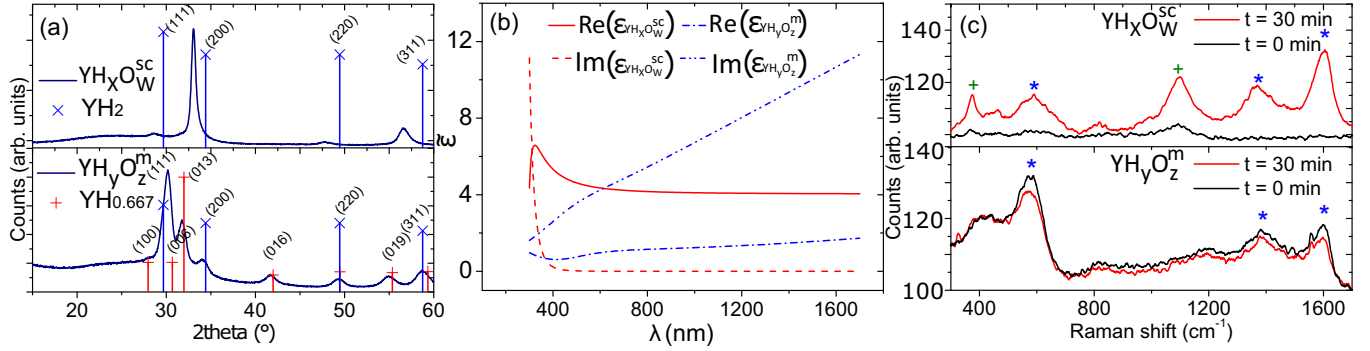
[*]jose.montero.amenedo@ife.no

FIG. 1. Characterization of the transparent-semiconducting $YH_xO_w^{sc}$ and opaque-metallic $YH_yO_z^m$ thin films: (a) GIXRD patterns, (b) real and imaginary components of the complex dielectric function $\tilde{\varepsilon}$ obtained by variable-angle ellipsometry, and (c) Raman measurements before and after 30 min illumination with an UV laser. As usual, λ signifies the wavelength of the incident light.

much higher than the one in the $YH_yO_z^m$ films. Indeed, an energy-dispersive x-ray spectroscopy analysis (EDS) of the equivalent samples deposited onto carbon substrates revealed an oxygen-yttrium atomic ratio of 1.29 and 0.40 for $YH_xO_w^{sc}$ and $YH_yO_z^m$, respectively. The reason why the films deposited at lower Γ contain less oxygen is still unclear, although it can be attributed to differences in the film porosity caused by the change in the partial pressure of the reactive gas (hydrogen) during the deposition process [13]. In summary, the GIXRD and EDS analysis revealed that the $YH_yO_z^m$ films contain less hydrogen, because they exhibit an hydrogen-deficient hexagonal phase ($YH_{0.667}$), but also less oxygen than the $YH_xO_w^{sc}$ films.

Figure 1(b) shows the real and imaginary components of the complex dielectric functions $\tilde{\varepsilon}_{YH_xO_w^{sc}}$ and $\tilde{\varepsilon}_{YH_yO_z^m}$ obtained for the $YH_xO_w^{sc}$ and $YH_yO_z^m$ films by variable angle spectroscopic ellipsometry. The determination of $\tilde{\varepsilon}_{YH_yO_z^m}$ and $\tilde{\varepsilon}_{YH_xO_w^{sc}}$ was achieved, as usual, by the fitting of the experimental ellipsometric angles Δ and Ψ to a theoretical model. Both the modeling and data fitting were performed by using the commercial software WVASE32 from J. A. Woollam Company, Inc. This software performs an iterative fitting to the experimental data by using the Marquardt-Levenberg algorithm [14]. In the case of the $YH_xO_w^{sc}$ films, a simple Cauchy model [15] combined with an Urbach tail (exponential) provided a good fitting to the experimental measurements, while for the $YH_yO_z^m$ films both Lorentz and Tauc-Lorentz oscillators [15] were considered.

Figure 1(c) shows the micro-Raman spectra corresponding to transparent-semiconducting $YH_xO_w^{sc}$ (upper panel) and opaque-metallic $YH_yO_z^m$ (lower panel) thin films, obtained by using a Horiba Jobin-Yvon LabRam Hr800 confocal microscope equipped with a 325 nm He-Cd laser set to a power density of 8×10^4 W cm^{-2}. Two scans were performed at different illumination times t. The first scan was performed as soon as the sample was placed under the laser probe, $t = 0$ min, and the second one after 30 min of laser exposure. The vibrational modes corresponding to the metallic $YH_yO_z^m$ films (centered at 590, 1302, and 1603 cm^{-1} and labeled with the $\star$ symbol) do not change as a function of illumination time. On the other hand, at $t = 0$ min the micro-Raman spectra for the wide-semiconducting $YH_xO_w^{sc}$ films present only two peaks (centered at 374 and 1096 cm^{-1} and labeled with the + symbol). After 30 min illumination, however, the peaks

attributed to the metallic phase ($\star$) are also observed in the $YH_xO_w^{sc}$ films. Moreover, after 30 min of laser exposure, the $YH_xO_w^{sc}$ films exhibited a dark spot, observed by the naked eye, in the region in which the laser probe was focused. This spot disappeared in a few minutes after switching off the laser.

The results in Fig. 1(c) suggest that the $YH_xO_w^{sc}$ films, in the photodarkened state, consist of a composite constituted by the $YH_xO_w^{sc}$ (clear) and $YH_yO_z^m$ phases. Assuming that the size of the $YH_yO_z^m$ inhomogeneity domains are much smaller than the wavelength of the incident light, the $YH_xO_w^{sc}$ (photodarkened) films will behave optically as a homogeneous medium of the *effective* complex dielectric function $\tilde{\varepsilon}_{eff}$ [16,17]. On this basis, the optical constants of the photodarkened $YH_xO_w^{sc}$ films can be approached by the Maxwell-Garnett effective medium theory, which is suitable for nanoparticle-dispersed composites in the dilute limit [17]. According to the Maxwell-Garnett theory, the effective complex dielectric function of the composite is described by [10]

$$\tilde{\varepsilon}_{eff} = \tilde{\varepsilon}_{YH_xO_w^{sc}} \frac{1 + \frac{2}{3}f\alpha}{1 - \frac{1}{3}f\alpha}, \tag{1}$$

where α is

$$\alpha = \frac{\tilde{\varepsilon}_{YH_yO_z^m} - \tilde{\varepsilon}_{YH_xO_w^{sc}}}{\tilde{\varepsilon}_{YH_xO_w^{sc}} + L(\tilde{\varepsilon}_{YH_yO_z^m} - \tilde{\varepsilon}_{YH_xO_w^{sc}})}, \tag{2}$$

f is the filling factor (i.e., volume fraction) of the $YH_yO_z^m$ phase, and L the depolarization factor. In this work the inhomogeneity domains have been considered to be spherical, therefore $L = \frac{1}{3}$. On the other hand, $\tilde{\varepsilon}_{YH_xO_w^{sc}}$ and $\tilde{\varepsilon}_{YH_yO_z^m}$ have been obtained previously and presented in Fig. 1(b).

Figure 2(a) shows the evolution of the experimental optical transmittance T versus illumination time t corresponding to the $YH_xO_w^{sc}$ films. In this case, the samples were illuminated by a broadband light source EQ-99XFC LDLS with an intense UV component, and the transmittance in the 300–1700 nm range was measured *in situ* by both Ocean Optics QE65000 and NIRQUEST512 spectrophotometers equipped with an integrating sphere. In addition, the calculated transmittance of the films—in the clear state at different stages of photodarkening—has been also included. The transmittance curves have been calculated by using the Fresnel equations for a thin film over a nonabsorbing substrate [18,19] and the
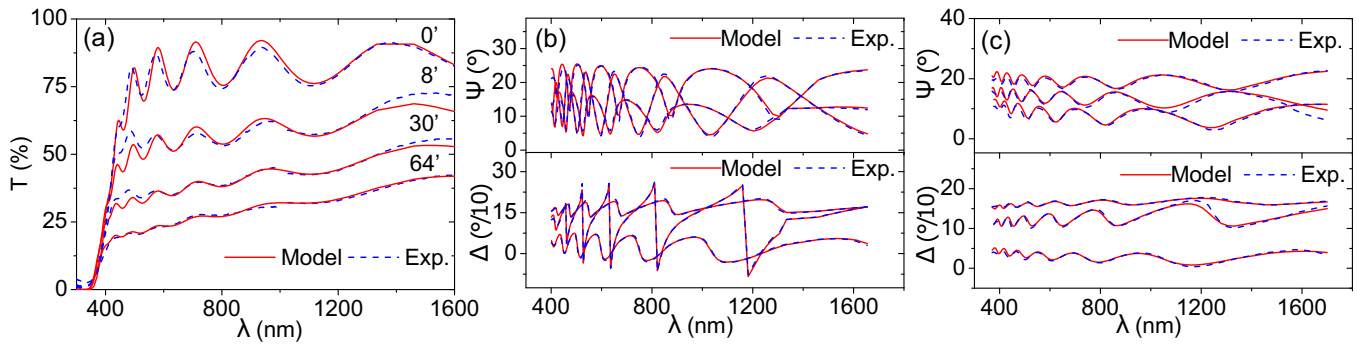
FIG. 2. The effective medium model reproduces very well the optical properties of the photochromic films $YH_xO_w^{sc}$ before and during illumination. (a) Transmittance curves T are shown after 0, 8, 30, and 64 min of illumination. The ellipsometric angles Ψ and Δ are shown (b) for the clear state and (c) after 64 min illumination. Ψ and Δ are shown for three angles of incidence, $50°$, $60°$, and $70°$. As usual, λ signifies the wavelength of the incident light.

effective dielectric function given by Eq. (1). As expected, the transmittance calculated for $f = 0$ (i.e., $\tilde{\varepsilon}_{eff} = \tilde{\varepsilon}_{YH_xO_w}$) matches very well the transmittance of the clear state ($t = 0$ min). Under illumination, the transmittance decreases gradually with time; the experimental transmittance of the $YH_xO_w^{sc}$ films after 8, 30, and 64 min of illumination corresponds to the one calculated for a $YH_xO_w^{sc}$(clear)/$YH_yO_z^m$ composite film with $f = 0.02$, 0.04, and 0.06, respectively (the dilute limit holds for these values of f). According to Fig. 2(a), small inclusions of the metallic phase $YH_yO_z^m$ in the $YH_xO_w^{sc}$ (clear) matrix can cause the big changes observed in the total transmittance of the film. For example, Fig. 2(a) shows that only 2% in volume of the metallic $YH_yO_z^m$ phase ($f = 0.02$) may cause a drop in the transmittance in the visible region of more than 30%.

The effective medium model also reproduces very well the gradual change of the ellipsometric angles Ψ and Δ during illumination. In this regard, the clear ($t = 0$ min) and photodarkened states ($t = 64$ min) are shown in Figs. 2(b) and 2(c), respectively. The ellipsometric spectra have been modeled considering a thin film of optical constants described by Eq. (1), assuming $f = 0.00$ for the clear state [Fig. 2(b)] and $f = 0.06$ for the photodarkened state [Fig. 2(c)]. For each case, the experimental and calculated angles Ψ (upper panel)

and Δ (lower panel) are shown for three different angles of incidence, $50°$, $60°$, and $70°$.

In summary, the optical properties of the photodarkened films can be explained quantitatively, according to the Maxwell-Garnett approximation, by the gradual formation of small metallic domains in the semiconducting lattice upon illumination. It is important to notice that the formation of small domains of the metallic phase (with a volume fraction of ∼0.06 or smaller) is able to cause a substantial decrease in the optical transmittance of the films. A similar situation was described by Giebels *et al.* in highly absorbing black Mg and rare-earth Mg switchable mirrors [20]. Although these results provide valuable hints, further investigations are needed in order to reach a complete understanding of the photochromic mechanism in oxygen-containing yttrium hydride thin films. Many questions remain open regarding this material, including why the darkening is reversible or which is the exact role and location of the oxygen atoms in the lattice.

[1] A. F. T. Hoekstra, A. S. Roy, T. F. Rosenbaum, R. Griessen, R. J. Wijngaarden, and N. J. Koeman, Phys. Rev. Lett. **86**, 5349 (2001).

[2] A. Ohmura, A. Machida, T. Watanuki, K. Aoki, S. Nakano, and K. Takemura, Appl. Phys. Lett. **91**, 151904 (2007).

[3] A. Ohmura, A. Machida, T. Watanuki, K. Aoki, S. Nakano, and K. Takemura, Phys. Rev. B **73**, 104105 (2006).

[4] J. N. Huiberts, R. Griessen, J. H. Rector, R. J. Wijngaarden, J. P. Dekker, D. G. de Groot, and N. J. Koeman, Nature (London) **380**, 231 (1996).

[5] T. Mongstad, C. Platzer-Björkman, J. P. Maehlen, L. P. Mooij, Y. Pivak, B. Dam, E. S. Marstein, B. C. Hauback, and

S. Z. Karazhanov, Sol. Energy Mater. Sol. Cells **95**, 3596 (2011).

[6] T. Mongstad, C. Platzer-Björkman, S. Z. Karazhanov, A. Holt, J. Maehlen, and B. Hauback, J. Alloys Compd. **509**, S812 (2011).

[7] A. Miniotas, B. Hjörvarsson, L. Douysset, and P. Nostell, Appl. Phys. Lett. **76**, 2056 (2000).

[8] C. V. Chandran, H. Schreuders, B. Dam, J. W. G. Janssen, J. Bart, A. P. M. Kentgens, and P. J. M. van Bentum, J. Phys. Chem. C **118**, 22935 (2014).

[9] J. Montero, F. A. Martinsen, M. Lelis, S. Z. Karazhanov, B. C. Hauback, and E. S. Marstein, Sol. Energy Mater. Sol. Cells (2017), doi: 10.1016/j.solmat.2017.02.001.

[10] J. C. Maxwell-Garnett, Philos. Trans. R. Soc. A **205**, 237 (1906).

[11] J. Garcés, J. Gervasoni, and P. Vajda, J. Alloys Compd. **404**, 126 (2005).

[12] A. Pishtshev and S. Z. Karazhanov, Solid State Commun. **194**, 39 (2014).

[13] J. Musil, P. Baroch, J. Vlček, K. Nam, and J. Han, Thin Solid Films **475**, 208 (2005).

[14] H. G. Tompkins, *WVASE32® Software Training Manual* (J. A. Woollam, Lincoln, NE, 2006), pp. 46–49.

[15] C. F. Klingshirn, *Semiconductor Optics* (Springer, Berlin, 2005).

[16] D. Aspnes, Thin Solid Films **89**, 249 (1982).

[17] G. A. Niklasson, C. G. Granqvist, and O. Hunderi, Appl. Opt. **20**, 26 (1981).

[18] M. Born, E. Wolf, A. Bhatia, D. Gabor, A. Stokes, A. Taylor, P. Wayman, and W. Wilcock, *Principles of Optics: Electromagnetic Theory of Propagation, Interference and Diffraction of Light* (Cambridge University Press, Cambridge, U.K., 2000).

[19] S. Bhattacharyya, R. Gayen, R. Paul, and A. Pal, Thin Solid Films **517**, 5530 (2009).

[20] I. A. M. E. Giebels, J. Isidorsson, and R. Griessen, Phys. Rev. B **69**, 205111 (2004).